Early mid-Holocene SST variability and surface-ocean water balance in the southwest Pacific

N. Duprey,[1] C. E. Lazareth,[1] T. Corrège,[2] F. Le Cornec,[1] C. Maes,[3] N. Pujol,[2] M. Madeng-Yogo,[1] S. Caquineau,[1] C. Soares Derome,[1] and G. Cabioch[1,4]

Received 23 May 2012; revised 28 September 2012; accepted 2 October 2012; published 17 November 2012.

[1] We present early mid-Holocene records of Sr/Ca, $\delta^{18}O$ and $\delta^{18}O_{sw}$ from marine archives collected in Vanuatu: two *Porites sp.* corals (6.7–6.5 ka BP) and a *Tridacna maxima* giant clam (6.2–6.0 ka BP). Sr/Ca, $\delta^{18}O$, and $\delta^{18}O_{sw}$ were used as proxies for sea surface temperature (SST) and sea surface salinity (SSS). The fossil geochemical records were compared to modern *Porites sp.* and *T. maxima* records. Reconstructed mean SSTs from the two fossil *Porites sp.* and from the modern coral are similar, implying that the Western Pacific Warm Pool (WPWP)' southern edge had reached its modern location by 6.7–6.5 ka BP. The post-glacial SST rise in the Southwest Pacific was thus completed by the early mid-Holocene. The two early mid-Holocene corals and the giant clam recorded saltier conditions than modern related to 1) a decoupling between the precipitation regime and the SPCZ due to a northerly position of this climatic feature and 2) an increase of the moisture transport to the extra-tropics, driven by a strengthened or extended Hadley cell. The longest $\delta^{18}O$ coral profile displays an El Niño Southern Oscillation (ENSO) signal reduced by 20–30% compared to the period 1928–1992, in concordance with the reduced ENSO variability observed in the Pacific area during the first half of the Holocene. However, the decoupling between the SPCZ and the precipitation regime may have also contributed to the weak ENSO signal recorded in the early mid-Holocene coral $\delta^{18}O$ profile.

Citation: Duprey, N., C. E. Lazareth, T. Corrège, F. Le Cornec, C. Maes, N. Pujol, M. Madeng-Yogo, S. Caquineau, C. Soares Derome, and G. Cabioch (2012), Early mid-Holocene SST variability and surface-ocean water balance in the southwest Pacific, *Paleoceanography*, *27*, PA4207, doi:10.1029/2012PA002350.

1. Introduction

[2] The transition from the early Holocene to the mid-Holocene (~7.0–6.0 ka BP) was accompanied by a progressive, but significant, change of the climate mean-state which took place at the millennial timescale. The early Holocene, that started at around 11 ka BP, was characterized by a cold post-glacial climate that warmed progressively until reaching temperature higher than modern ones during the Holocene Thermal Maximum, at around 9.0–5.0 ka BP [see the review proposed by *Renssen et al.*, 2012]. During the first part of the Holocene the summer insolation in the Northern Hemisphere was higher than present conditions as a response to the orbital forcing [*Berger and Loutre*, 1991]. This strong insolation resulted in higher monsoon activity in Africa [*deMenocal et al.*, 2000] and in Asia [*Zhang et al.*, 2011]. During the mid-Holocene period, that started ca. 7.0–6.0 ka BP, the boreal summer insolation decrease [*Berger and Loutre*, 1991] and the monsoon regimes weakened [*Wang et al.*, 2005; *Wanner et al.*, 2008; *Zhang et al.*, 2011]. Superimposed to these changes, occurring at the millennial time-scale, the mid-Holocene also witnessed the strengthening of the more prominent high frequency climatic variability mode: the El Niño Southern Oscillation – ENSO [e.g., *Haberle et al.*, 2001; *Sandweiss et al.*, 2001; *Tudhope et al.*, 2001; *Moy et al.*, 2002; *Gagan et al.*, 2004; *Koutavas et al.*, 2006; *Vargas et al.*, 2006]. ENSO is associated with dramatic changes in the precipitation regime and sea surface temperature (SST) throughout the world, leading to ecological and socio-economical disasters [e.g., *Lyon*, 2004; *Cane*, 2005; *McPhaden et al.*, 2006]. The heart of this climatic oscillation is nested in the Pacific Ocean; however ENSO' influence extends beyond the Pacific boundaries and reaches remote areas through strong teleconnections [*Kiladis and Diaz*, 1989; *Ambrizzi et al.*, 1995; *Diaz et al.*, 2001].

[3] Improving predictability of the ENSO evolution represents a major challenge for the coming decades; this goal requires refining our understanding of the links between

[1]IPSL/LOCEAN, UPMC/CNRS/MNHN, IRD France Nord, France.
[2]Université Bordeaux, EPOC UMR 5805, Talence, France.
[3]LEGOS, UMR 5566, Institut de Recherche pour le Développement, Toulouse, France.
[4]Deceased 2011.

Corresponding author: N. Duprey, Institut de Recherche pour le Développement, 32 Ave. Henri Varagnat, FR-93140 Bondy, France. (nicolas_duprey@yahoo.fr)

0883-8305/12/2012PA002350

ENSO variability and the changes in the climatic mean-state as well as improving climate simulations based on numerical models. Early mid-Holocene climatic changes present the same order of magnitude as the ongoing climate changes. Documenting such changes will provide thus invaluable clues to understand the mechanisms involved in the climate dynamic. However, the spatial and the temporal resolution of the early mid-Holocene paleoclimatic reconstructions are still insufficient to fulfill such an objective.

[4] The Southwest (SW) Pacific area is a key-region of the Pacific Ocean to track past climate changes. Indeed, the SW Pacific climate is governed by two major climatic structures that influence the global climate: the Western Pacific Warm Pool (WPWP) and the South Pacific Convergence Zone (SPCZ). ENSO strongly influences the position and size of both the WPWP and SPCZ at the interannual timescale [e.g., *Vincent*, 1994].

[5] The WPWP can be defined as the permanent body of warm seawater located to the east of a line between the Philippines and Papua New Guinea (PNG), excluding the warm waters within the Indonesian Archipelago. This warm water body causes a strong atmospheric convection over the SW Pacific, influencing the global distribution of heat and water evaporation [*Cane and Clement*, 1999]. To date, the exact definition of the spatial extent of the WPWP has been elusive as the warm pool margins are not solely defined by a specific SST front, but rather by distinct hydrological features and ecosystem dynamics [*Picaut et al.*, 2001; *Le Borgne et al.*, 2002; *Maes et al.*, 2010]. Nevertheless, the WPWP area is usually defined as the water body enclosed within the 28°C SST isotherm [*Wyrtki*, 1989].

[6] The SPCZ is the largest extension of the Inter-Tropical Convergence Zone – ITCZ [*Trenberth*, 1976; *Kiladis et al.*, 1989; *Vincent*, 1994]. The SPCZ is a band of low-level convergence, cloudiness and precipitation, present all year-long, characterized by warm SST and low sea surface salinity (SSS). The SPCZ is generally defined as the maximum precipitation tongue extending southeastward from PNG and the Solomon Islands down to the south of French Polynesia.

[7] SSS and SST thus represent key-variables to assess the variability of these climatic features in terms of location and activity. The geochemical composition of massive coral skeleton and giant clam shell is sensitive to changes occurring in the surrounding seawater. Past changes in sea surface conditions can thus be assessed from the geochemical composition of coral and giant clam fossil specimens. The strontium-calcium (Sr/Ca) ratio of coral skeleton is now widely used as a paleothermometer [e.g., *Swart*, 1981; *Schneider and Smith*, 1982; *Beck et al.*, 1992; *Corrège*, 2006]. Concerning giant clams, the Sr/Ca composition of the shell is influenced by vital effects, hampering the use of this ratio as a paleothermometer [*Elliot et al.*, 2009].

[8] Stable oxygen isotopes composition ($\delta^{18}O$) of coral skeleton and giant clam shell is a function of both temperature and oxygen isotopic composition of the surrounding water ($\delta^{18}O_{sw}$) [*McConnaughey*, 1989]. In regions dominated by strong atmospheric convection, as in the SW Pacific area, the $\delta^{18}O_{sw}$ is a reliable proxy of SSS since both SSS and $\delta^{18}O_{sw}$ depend on the surface-ocean water balance, i.e., the evaporation/precipitation balance [*Morimoto et al.*, 2002; *Kilbourne et al.*, 2004; *Juillet-Leclerc et al.*, 2006]. Obtaining Sr/Ca and $\delta^{18}O$ profiles from coral and giant clam can thus provide useful information on the size and location of the WPWP and of the SPCZ.

[9] Early mid-Holocene SST and $\delta^{18}O_{sw}$ monthly resolved data sets have been reconstructed from Sr/Ca and $\delta^{18}O$ records obtained from two fossil *Porites sp.* coral colonies and a fossil *Tridacna maxima* giant clam from Vanuatu archipelago (SW Pacific). These data are compared to modern records based on a *Porites sp.* colony from Vanuatu and a modern specimen of *T. maxima* from New Caledonia (SW Pacific). Based on these comparisons, the early mid-Holocene climate variability in the SW Pacific is documented, focusing first on the post-glacial SST evolution in this area and its implications in terms of WPWP' southern edge location. Then, the surface-ocean water balance variability is investigated to study the seasonal influence of the SPCZ in the SW Pacific area. Finally ENSO variability is presented and discussed.

2. Climatic Setting

[10] The climate in the SW Pacific (Figure 1) is mainly influenced by the seasonal extension of the WPWP southern edge and of the SPCZ (Figure 2). During the austral summer, the WPWP and the SPCZ move southward, bringing warmer and fresher waters in this region (linked to precipitation increase). The northward migration of the WPWP and the SPCZ during the austral winter results in cooler and saltier (less precipitation) waters. In Vanuatu, seasonal variations of SSS and SST are thus anti-correlated (Figure 3). Because of its southern location compared to Vanuatu, New Caledonia is less influenced by the WPWP southern edge and by the SPCZ. This explains the differences with the Vanuatu SST and SSS data in terms of mean values and seasonal cycle amplitude (Figure 3).

[11] In the SW Pacific, interannual climatic variability is influenced by ENSO. During an El Niño event, the southern edge of the WPWP and the SPCZ both move northward of their mean position, resulting in cooler and saltier conditions in Vanuatu. During a La Niña event, the WPWP and the SPCZ migrate southward of their mean position, bringing warmer and fresher conditions. An anomalous decrease (increase) in SST associated with an anomalous decrease (increase) in SSS indicates thus La Niña (El Niño) phase of ENSO. In the SW Pacific area, precipitation, and thus SSS, variations present a higher correlation with ENSO than SST (Figure 2).

3. Materials and Methods

3.1. Fossil Material

[12] For this study, fossil corals and giant clams that grew in a shallow fringing reef environment were targeted. Fossils specimens were collected on uplifted fringing reef areas of Espiritu Santo Island (15.35°S, 167.18°E), the main island of the Vanuatu archipelago. Two fossil *Porites sp.* colonies, Psp-06-09 and Psp-07-09, were collected on an islet (Ratua Island) located in the southeast of Espiritu Santo (Figure 1). The length of the colonies was 29 cm and 35 cm along the growth axis. Psp-07-09 is composed of two slabs. One of these slabs presents a growth stop, marked with a one-millimeter layer of altered skeleton, causing a temporal hiatus. The left valve of a *Tridacna maxima* giant clam was recovered on the Southeast part of Espiritu Santo Island (Figure 1). This sample, labeled

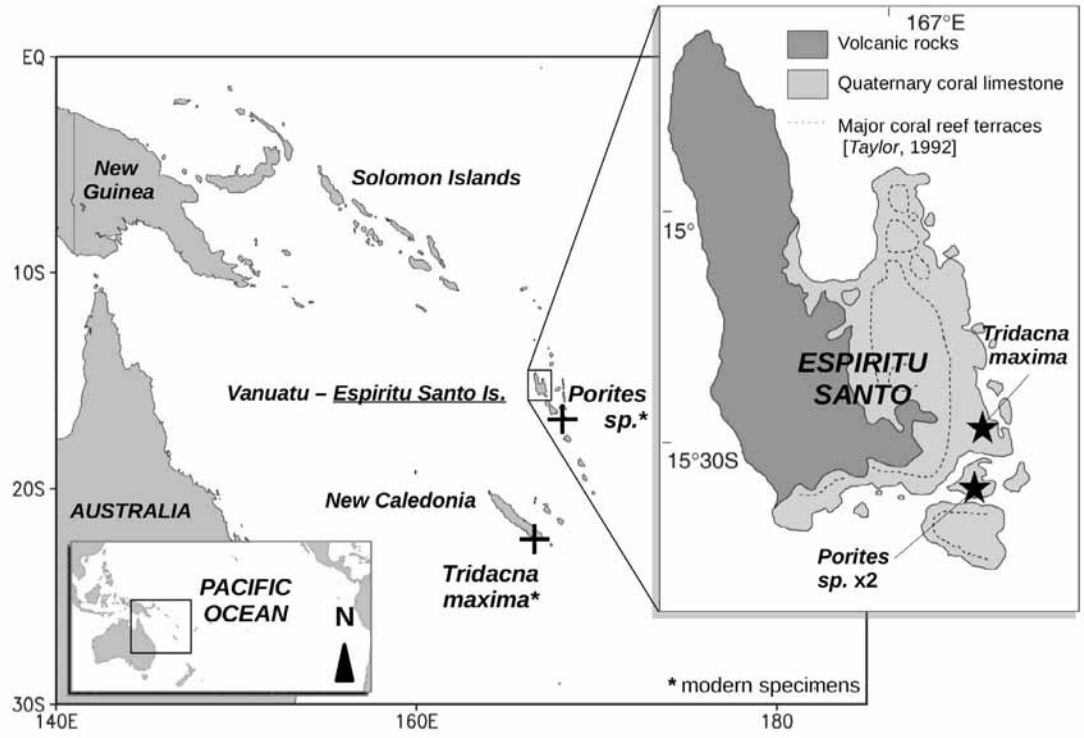

Figure 1. Location of New Caledonia and of the Vanuatu archipelago in the Southwest Pacific. Crosses: sampling sites of the modern specimens. The insert shows a detailed map of the Espiritu Santo Island with the collection sites of the fossil material (stars). Uplifted coral reef data is from *Taylor* [1992].

T-10-09, measured 25.5 cm along the antero-posterior axis and 16.5 cm along the dorso-ventral axis.

3.2. Modern Material and SST/SSS Data Sets

[13] To define a modern baseline against which to compare the fossil records, a *Tridacna maxima* and a *Porites sp.* modern colony were collected in New Caledonia and in Vanuatu respectively. These two sites were described in terms of averaged values and seasonal variations of instrumental SST and SSS.

[14] 3.2.1. *New Caledonia* – A modern *Tridacna maxima* was collected alive in 2008, on the *Fausse Passe de Uitoé* reef (22.28°S, 166.98°E – New Caledonia – Figure 1). This giant clam (T-02-08) grew then in a seawater-fed aquarium at the *Aquarium des Lagons* (Nouméa, New Caledonia) for 13 months. The seawater feeding the aquarium was continuously pumped from a coastal fringing reef nearby the aquarium. Modern conditions in New Caledonia were characterized using SST and SSS records extending from 1992 to 2009. These data were measured on the clam collection site (*Fausse Passe de Uitoé* reef) and were provided by the *Réseau d'observation des stations côtières* of the *Institut de Recherche pour le Développement* (IRD-Nouméa, New Caledonia).

[15] 3.2.2. *Vanuatu* – A modern living *Porites sp.* colony (VA-EPI) was collected in 2007 on a fringing reef of the Epi Island in Vanuatu (Figure 1). The $\delta^{18}O$ record from a modern *Porites lutea* that grew from 1928 to 1992 on Espiritu Santo [*Kilbourne et al.*, 2004] was also used to assess possible changes in ENSO variability during the early mid-Holocene. Modern SSS conditions in Vanuatu were taken from the data set compiled by *Gouriou and Delcroix* [2002], on a 2° × 2° grid centered on 16°S–165.5°E, for the 1949–2008 period. The HadISST1.1 data set was used to characterize the modern SST in Vanuatu [*Rayner et al.*, 2003]. Data were selected for the period 1970–2011 on a 3° × 3° grid, centered on 15.5°S–164.5°E.

3.3. Dating and Preservation of the Fossil Samples

[16] Fossil samples were dated using conventional ^{14}C measurements and dates were calibrated using the Marine09 database [*Reimer et al.*, 2009]. The DeltaR value used for the Vanuatu area was 29 ± 28 years according to *Petchey et al.* [2008]. The coral samples and the fossil giant clam shell were screened for their mineralogical composition and micro-structure preservation before geochemical analysis to ensure they were well-preserved. Mineralogical analyses were carried out using X-ray diffraction (XRD) on a Siemens® D500 device (Cu-Kα, 40 kV, 30 mA) with a scan velocity of two seconds at a step size of 0.02° 2θ. Minerals were identified by comparison with the reference JCPDF database (Joint Committee of Powder Diffraction File). The preservation state of the fossil specimens was evaluated by comparing Scanning Electronic Microscopy (SEM) images of modern and fossil specimens of coral and giant clams. Samples were sputter-coated with platinum and observed on a Cambridge® S360 device at 15 kV.

3.4. Geochemical Sampling

[17] 3.4.1. *Coral samples* - Corals were cut in 10 mm-thick slabs parallel to the major growth axis. X-radiographs revealed the annual density banding. A couple of high- and low-density bands was assumed to represent one year of

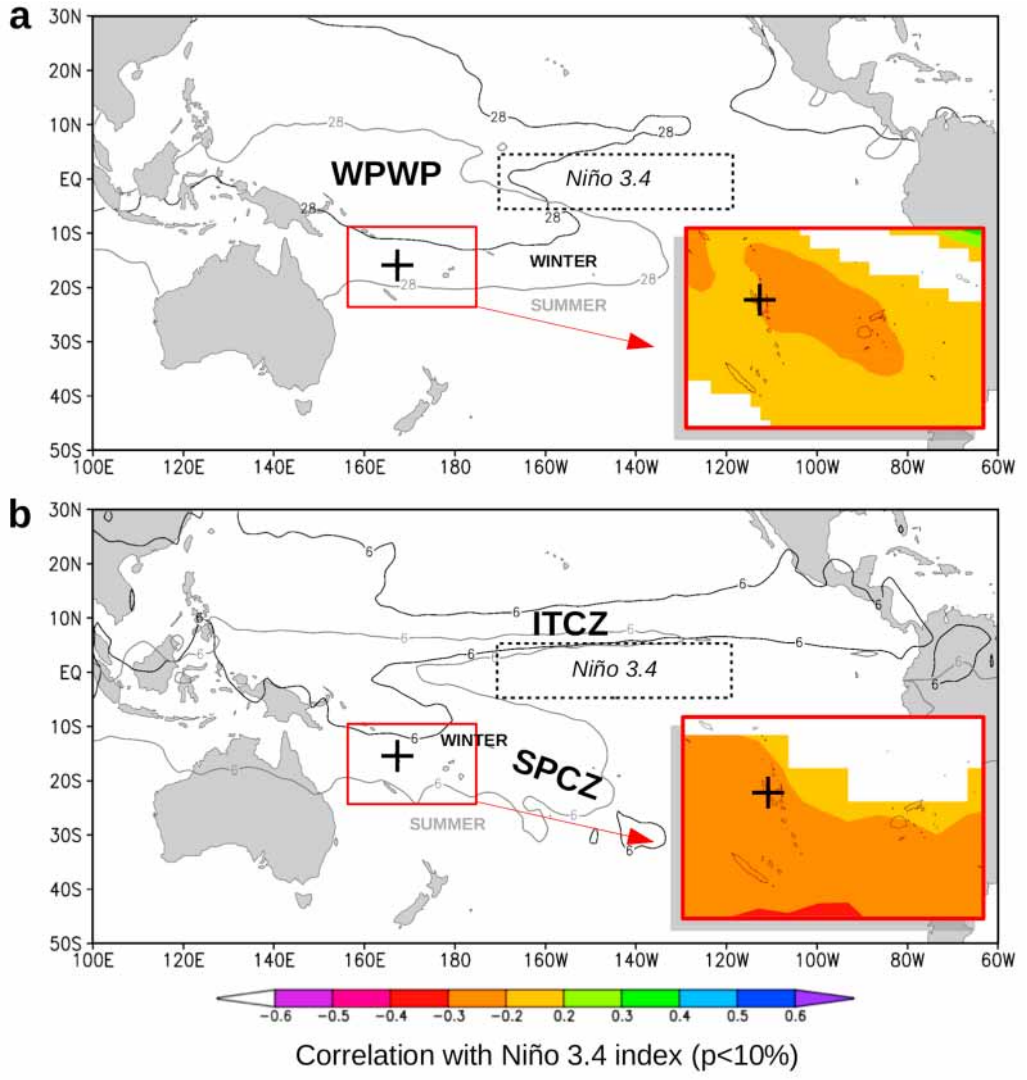

Figure 2. Seasonal location of the main climatic features of the Pacific Ocean: (a) The Western Pacific Warm Pool (WPWP). The gray (black) curve represents the 28°C isotherm in winter (summer) (HadISST1 mean 1980–2011 period, [*Rayner et al.*, 2003]). The insert shows the Pearson correlation coefficient (r) between the SST data set (same as above) and the SST in the El Niño 3.4 box for the SW Pacific area. (b) The Inter-Tropical Convergence Zone (ITCZ) and the South Pacific Convergence Zone (SPCZ). The gray (black) curve represents the 4 $mm.d^{-1}$ isohyet in winter (summer) (CMAP 1980–2010). The insert shows the Pearson correlation coefficient (r) between the precipitation data set (same as above) and the SST in the El Niño 3.4 box for the SW Pacific area. Black cross: Vanuatu archipelago. Modified from Climate Explorer (http://climexp.knmi.nl).

coral growth [*Knutson*, 1972]. Before sampling, coral slabs were cleaned in milli-Q water in an ultrasonic bath and oven-dried at 40°C. Coral slabs were sampled continuously along the main growth axis with a step of 1 mm with a diamond drill-bit using a three-axis positioning system.

[18] 3.4.2. *Giant clam samples* – The central ridge of the modern (T-02-09) and of the fossil (T-10-09) *Tridacna maxima* left valves were cut off with a diamond saw. For oxygen stable isotope analyses, samples were obtained using a Micro-Mill device (New Wave®). Samples were milled following growth increments in the outer shell layer, every 0.25 mm (modern) and 0.80 mm (fossil). The modern giant clam was sampled on the part of the shell deposited from September 2008 to October 2009 while the specimen was in the aquarium.

3.5. Geochemical Analysis and Data Processing

[19] 3.5.1. *Strontium/Calcium* – The Strontium (Sr) and Calcium (Ca) concentrations of coral samples VA-EPI, Psp-06-09, and Psp-07-09 were determined following the method detailed by *Le Cornec and Corrège* [1997]. Analyses were made using an inductively coupled plasma mass spectrometer (ICP-MS; Agilent 7500 CX®). The certified reference material JCp-1 (coral material) from the Geological Survey of Japan [*Okai et al.*, 2002; *Inoue et al.*, 2004; *Hathorne et al.*, 2010] was used to validate the accuracy of the

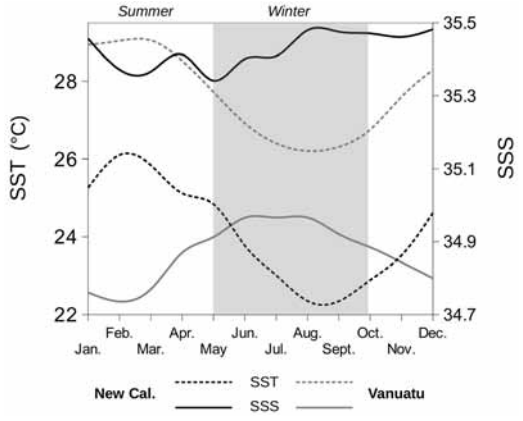

Figure 3. Instrumental SST and SSS data. The modern SST and SSS conditions in New Caledonia were recorded by a thermo-salinograph located on the *Fausse Passe de Uitoé* reef (22.28°S, 166.98°E), from 1992 to 2009. Data were provided by the *Réseau d'observation des stations côtières* of the Institut de Recherche pour Développement (IRD-Nouméa, New Caledonia). Vanuatu SSS data for the 1949 to 2008 period came from a 2° × 2° grid, centered on 16°S, 165.5°E [*Gouriou and Delcroix*, 2002]. SST data was selected for the period 1970–2011 on a 3° × 3° grid, centered on 15.5°S, 164.5°E (HadISST1.1) [*Rayner et al.*, 2003].

analyses. Analytical reproducibility (1σ) on coral Sr/Ca measurements was 0.05 mmol.mol^{-1}, based on 30 runs of a home-made coral standard on a six-month period. Time was assigned to the coral geochemical profiles based on both Sr/Ca ratio and density banding. Considering that today lower (higher) SST is found in August (February) in Vanuatu, the highest (lowest) Sr/Ca values were arbitrary set as August (February - Figure 3). Each so-obtained time series was then mathematically re-sampled at a monthly resolution by linear interpolation. To avoid any data smoothing that could result from the interpolation process, the re-sampling was made by interpolating six points between each Sr/Ca minima/maxima pairs, assuming that coral growth is linear within six-month periods.

[20] 3.5.2. $\delta^{18}O$ - The oxygen stable isotope samples of the modern *Porites sp.* (VA-EPI), the fossil *Porites sp.* (Psp-07-09), and the two *Tridacna maxima* (T-02-08 and T-10-09) were analyzed on a GV IsoPrime® mass-spectrometer at LOCEAN (Paris 6 University), whereas fossil *Porites sp.* Psp-06-09 was analyzed on a GV Optima® mass-spectrometer at EPOC (Bordeaux I University). Both instruments were coupled to a Multiprep carbonate Gilson®.

[21] To ensure the inter-spectrometer comparison, 70 duplicates samples of Psp-07-09 were analyzed on both equipments. Results are expressed as δ^{18}O (standardized against Vienna Peedee Belemnite - vpdb). The analytical precision (1σ) on oxygen isotopic determinations, based on 10 runs of the reference material NBS-19, was 0.08‰ vpdb within one day, for both spectrometers. Time was assigned to the δ^{18}O profiles based on the tie-points determined previously from the Sr/Ca ratio and the density banding. Each time series was mathematically re-sampled as previously described.

[22] 3.5.3. $\delta^{18}O_{sw}$ – The $\delta^{18}O_{sw}$ values were calculated from the coral Sr/Ca and the δ^{18}O records using the equation established by *Juillet-Leclerc and Schmidt* [2001]: $\delta^{18}O_{aragonite} - \delta^{18}O_{sw} = 0.45 - 0.20$*SST (Sr/Ca was converted into SST using the mean equation for *Porites sp.* [*Corrège*, 2006]). Mean seasonal cycles of Sr/Ca and $\delta^{18}O_{sw}$ were calculated for all coral records by averaging each monthly re-sampled value (e.g., average of all January values, all February values, etc.). Most of the monthly $\delta^{18}O_{sw}$ values, excluding the seasonal peak values, were averaged to obtain a mean surface ocean water balance. Seasonal extremes below the mean surface ocean water balance reflect a freshening of the superficial waters and extremes above the mean define a salinity increase in the superficial waters.

[23] 3.5.4. *ENSO frequency band-pass filtering* – The δ^{18}O profiles of the modern coral of *Kilbourne et al.* [2004] and of the continuous fossil coral record Psp-06-09 were band-pass filtered as described by *Tudhope et al.* [2001]. This process extracts the 2.5- to 7-yr frequency of the signal (i.e., the dominant mode of modern ENSO - [*Trenberth*, 1976]). First, the modern coral δ^{18}O record was compared with to the 2.5–7 years band-pass filtered El Niño 3.4 index [*Kaplan et al.*, 1998] to ensure that the ENSO variability was faithfully recorded. Second, the ENSO variability was quantified by calculating the standard deviation of the modern and fossil band-pass filtered δ^{18}O time series. To assess possible changes in ENSO variability during the early mid-Holocene compared to modern conditions, the standard deviation of the 25-yr long fossil ENSO record was compared to the standard deviation of the modern ENSO record calculated on different time periods lasting approximately 20 years: 1928–1950, 1951–1970, and 1971–1992.

4. Results

4.1. Samples Dating and Preservation

[24] The two *Porites sp.* colonies were dated at 6.7–6.5 ka BP (see Table 1 for ^{14}C ages). The fossil *Tridacna maxima* was dated at 6.2–6.0 ka BP. XRD analyses revealed that the three coral samples (modern and fossils one) and the fossil

Table 1. Main Geochemical Characteristics of the Samples Presented in This Study[a]

Archive	*Tridacna maxima*		*Porites sp.*		
Reference	T-02-09	T-10-09	VA EPI	Psp-06-08	Psp-07-08
Date ^{14}C (yr. BP ± uncert.)	*modern*	5737 ± 27	*modern*	6208 ± 35	6220 ± 32
Date cal (yr. BP − 2σ range)	—	6.2–6.0	—	6.7–6.5	6.7–6.5
Location	New Caledonia	Vanuatu	Vanuatu	Vanuatu	Vanuatu
Record length (yr.)	1	6	7	25	19
δ^{18}O (vpdb ‰)	−1.04 ± 0.53	−0.99 ± 0.33	−4.68 ± 0.21	−4.35 ± 0.16	−4.29 ± 0.28
$\delta^{18}O_{sw}$ (vpdb ‰)	—	—	0.01 ± 0.05	0.27 ± 0.05	0.28 ± 0.04
Sr/Ca (mmol mol^{-1})	—	—	8.99 ± 0.09	9.01 ± 0.08	9.03 ± 0.08

[a]Geochemical mean values are calculated from monthly re-sampled time series.

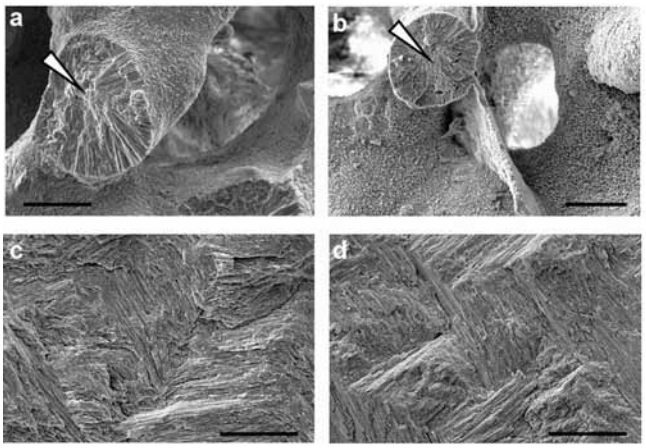

Figure 4. Microstructural comparison between modern and fossil (this study) corals and giant clam (SEM images, scale: 50 μm). Massive coral *Porites sp.* specimens: (a) modern coral VA EPI; (b) early mid-Holocene coral Psp-07-09, with arrow indicating center of calcification. Giant clam *Tridacna maxima* specimens: (c) modern giant clam T-02-09; (d) early mid-Holocene giant clam T-10-09 (scale 50 μm).

giant clam are composed of 100% aragonite. Comparison of SEM images of modern and fossil specimens revealed that the fossil material is well-preserved. Indeed, the fossil corals present unaltered primary aragonite needles and the centers of calcification are affected neither by dissolution nor by secondary aragonite deposition (Figure 4a and 4b). The crossed-lamellar aragonitic micro-structure of the giant clam outer shell layer is also well-preserved (Figure 4c and 4d).

4.2. Coral Growth Stop

[25] A one-millimeter layer of altered skeleton, interpreted as a growth stop, was observed on one slab of the fossil Psp-07-09 #2. On this particular section of the skeleton, sponge chips were observed (SEM study). This confirms that this part of the colony suffered tissue loss during a short period. The density banding pattern, $\delta^{18}O$, $\delta^{18}O_{sw}$, and Sr/Ca records of this slab present annual variations, except for a 4-cm part that overgrew the growth stop. Time could not be assigned for the geochemical profiles in that 4-cm thick section, these data are not included in the study (shaded area in Figure 5).

4.3. Coral Records

[26] Comparison of the density banding and of the geochemical profiles revealed that the Psp-06-09 record is 25 years long and the Psp-07-09 record is 19 years long. The $\delta^{18}O$ reproducibility obtained from the samples analyzed twice, i.e., on the two different mass spectrometers, is good (mean relative error = 3%, n = 48), excluding analytical bias that could have been due to the use of two different equipment. Psp-06-09 and Psp-07-09 $\delta^{18}O$ records have a similar mean $\delta^{18}O$ (Table 1). The modern coral VA-EPI from Vanuatu recorded a 7 year period (1999 to 2006 - Figure 5). The Sr/Ca composition of the modern coral reflects the mean SST, which was 27.7 $\pm$ 1.1°C for the 1970–2011 period (SSS was 34.9 $\pm$ 0.3 – 1949–2008, based on the PSS-78 scale). The fossil Sr/Ca mean values are similar to the modern mean (9.00 mmol.mol^{-1}).

[27] The skeletal Sr/Ca, $\delta^{18}O$, and $\delta^{18}O_{sw}$ time series generated from the fossil corals (Psp-06-09 and Psp-07-09)

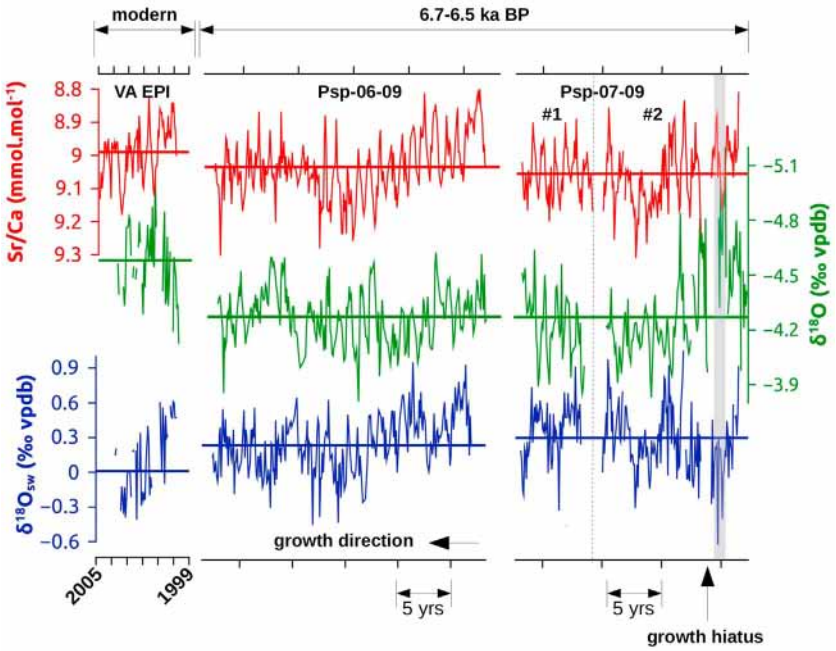

Figure 5. Monthly resolved geochemical data obtained from the modern and the two fossil *Porites sp.* corals from Vanuatu: Sr/Ca (red), $\delta^{18}O$ (green) and $\delta^{18}O_{sw}$ (blue). The thick horizontal line represents the average value of each record. The growth hiatus of the colony Psp-07-09 is showed by the black arrow and the shaded area indicates the anomalous part of the record not included in the study (cf. text). Note that both Sr/Ca-axis and $\delta^{18}O$-axis are inverted.

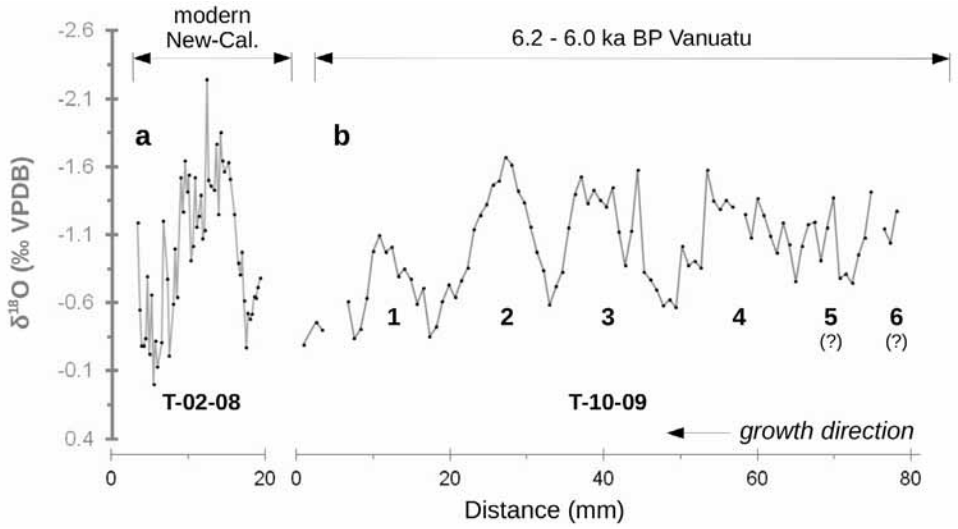

Figure 6. $\delta^{18}O$ records obtained from the modern and the fossil *Tridacna maxima* giant clams as a function of distance (zero corresponds to the animal death). The $\delta^{18}O$ axis is inverted. (a) Record obtained from the modern *T. maxima* T-02-09 collected in New Caledonia and (b) record of the 6.2–6.0 ka BP *T. maxima* collected in Vanuatu.

all display seasonal variations (Figure 5). The Sr/Ca records of the modern and of the two early mid-Holocene corals have a mean value of ~9.00 mmol.mol^{-1} (Table 1, Figure 5). The two fossil $\delta^{18}O$ ($\delta^{18}O_{sw}$) records have similar mean values and are ^{18}O-enriched by +0.3‰ vpdb (+0.3‰ vpdb) compared to the modern record (Table 1, Figure 5).

4.4. Giant Clam Records

[28] The $\delta^{18}O$ composition of the modern *Tridacna maxima* from New Caledonia shows one annual cycle corresponding to the 13 months spent in the aquarium – September 2008 to October 2009 (Figure 6a). The mean $\delta^{18}O$ composition of this specimen is -1.04 ± 0.53‰ vpdb. This value reflects the mean SST and SSS conditions in New Caledonia today: average SST and SSS values recorded in the period 1992–2009 are 24.1 ± 1.6°C and 35.4 ± 0.22 (based on the PSS-78 scale) respectively. The $\delta^{18}O$ composition of the modern *T. maxima* is used as a baseline for modern conditions against which to compare the $\delta^{18}O$ composition of the early mid-Holocene *T. maxima*. The $\delta^{18}O$ record from the fossil *T. maxima* is characterized by four clear annual cycles and two less defined cycles (Figure 6b). The 6.2–6.0 ka BP *T. maxima* record from Vanuatu has a mean $\delta^{18}O$ value of −0.99‰ vpdb which is similar to the modern specimen from New Caledonia (Table 1).

4.5. Seasonal Variability From the Coral Records

[29] The modern coral Sr/Ca record (Figure 7a) displays seasonal variations that reflect well the instrumental SST variations measured in Vanuatu (Figure 3). The modern coral recorded low $\delta^{18}O_{sw}$ values oscillating around 0‰ vpdb during most part of the year, excepted of a $\delta^{18}O_{sw}$ peak reaching 0.3‰ vpdb in October (Figure 7a). The $\delta^{18}O_{sw}$ data

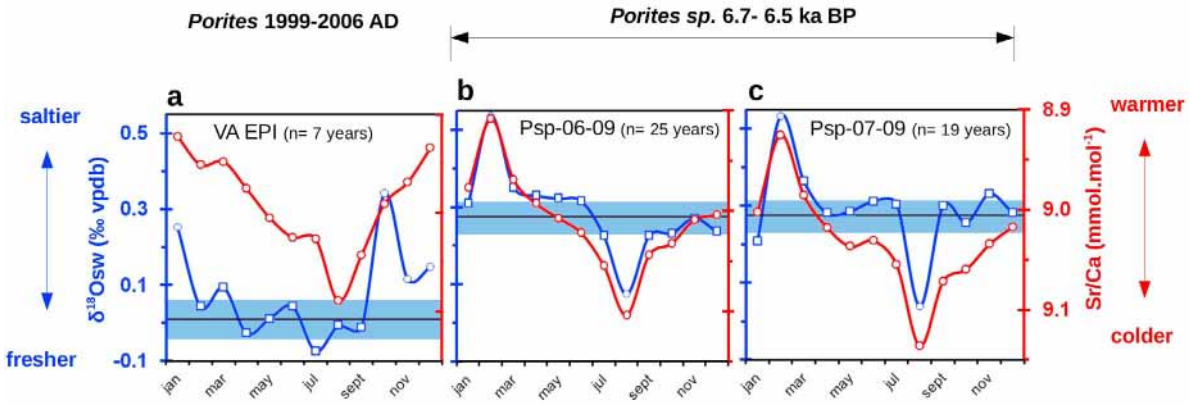

Figure 7. Seasonal variations of Sr/Ca (red) and $\delta^{18}O_{sw}$ (blue) from corals collected in Vanuatu. The average $\delta^{18}O_{sw}$ (black line and 1σ standard deviation interval in blue) was calculated by averaging the data points represented by (a) the squares (i.e., extremes not included), (b) modern coral record, and (c) 6.7–6.5 yrs BP fossil coral colonies.

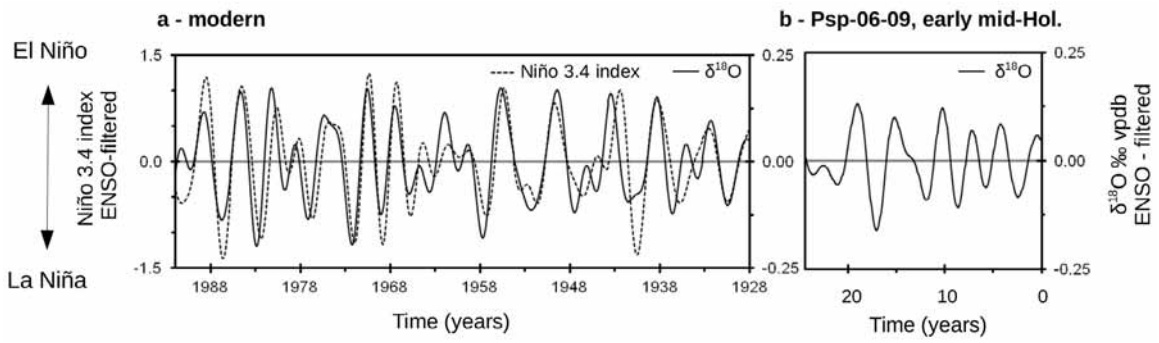

Figure 8. Comparison of modern versus early mid-Holocene ENSO amplitudes. (a) ENSO-filtered modern coral $\delta^{18}O$ data [data from *Kilbourne et al.*, 2004] and El Niño 3.4 Index. (b) *Porites sp.* Psp-06-09 ENSO-filtered $\delta^{18}O$ data.

recorded well the SSS signal with low salinity conditions all yearlong, excepted in winter, that reflect well the seasonal patterns observed today in Vanuatu (Figure 3).

[30] The two early mid-Holocene coral records display almost identical seasonal Sr/Ca and $\delta^{18}O_{sw}$ variations. The two early mid-Holocene Sr/Ca records have amplitudes similar to that of the modern Sr/Ca record (Figure 7). The $\delta^{18}O_{sw}$ cycle recorded by the fossil coral is characterized by a rather flat profile centered around 0.3‰ vpdb with a positive peak reaching 0.5‰ vpdb in February and a negative peak reaching 0.0‰ vpdb in August (Figure 7b and 7c). Unlike the modern coral records, the two early mid-Holocene coral colonies revealed saltier summer and fresher winter conditions. The consistency of the Sr/Ca and the $\delta^{18}O_{sw}$ profiles in the two fossil records indicates that the synchronous seasonal variation of SST and SSS is a robust feature of the early mid-Holocene.

4.6. ENSO Variability

[31] The ENSO-filtered $\delta^{18}O$ data of the modern coral [*Kilbourne et al.*, 2004] correlates well with the ENSO-filtered El Niño 3.4 index (Figure 8a), indicating that the Vanuatu modern coral recorded faithfully the ENSO variations. The amplitude of the filtered 25-years long $\delta^{18}O$ profile of the fossil coral Psp-06-09 is slightly lower than the modern record (Figure 8b). The standard deviation of the 25-yr long fossil record is equal to 0.067. This value was compared to the standard deviation of the modern ENSO-filtered $\delta^{18}O$ record calculated over three distinct periods: 1928–1950 (sd = 0.081), 1951–1970 (sd = 0.088) and 1971–1992 (sd = 0.097). The variability of the early mid-Holocene record is respectively 17%, 24%, and 31% lower than the modern ENSO signal recorded during these three periods.

5. Discussion

5.1. Post-Glacial SST Rise in the Southwest Pacific

[32] The mean Sr/Ca values of the two fossils and of the modern coral colonies from Vanuatu indicate that the early mid-Holocene mean SST was similar to its modern value (Figure 5). Considering the analytical error on strontium-calcium analyses (± 0.05 mmol.l^{-1}) and the average coral Sr/Ca versus temperature slope (-0.0607 mmol.l^{-1}.°C^{-1} [*Corrège*, 2006]), the accuracy of the Sr/Ca paleothermometer is ± 1°C within the analytical settings of this study. Mean SST gridded instrumental data is ~28°C in Vanuatu implying that the reconstructed early mid-Holocene mean SST was between 27 and 29°C.

[33] In the SW Pacific area, SST reconstructions from coral Sr/Ca and $\delta^{18}O$ giant clam archives revealed cooler conditions than present until ca. 7.0 ka BP [*Aharon*, 1980; *Beck*, 1997; *Abram et al.*, 2009]. Cooler SSTs in the early Holocene are supposedly linked to the delayed SW Pacific post-glacial SST rise [*Beck*, 1997; *Gagan et al.*, 2004]. Our results show that the post-glacial SST rise was completed by the early mid-Holocene in the SW Pacific. This observation is in agreement with the slightly warmer SST reported from other coral records from New Caledonia [*Montaggioni et al.*, 2006] and in the Australian Great Barrier Reef [*Gagan et al.*, 1998, 2004]. All these coral records, support the hypothesis of a moderate warming of the equatorial Western Pacific during the "Holocene Thermal Maximum" (ca. 8–7 ka BP), as it is also suggested by marine sediment records [*Stott et al.*, 2004] and by global atmosphere-ocean-vegetation model simulations [*Renssen et al.*, 2012].

5.2. Short-Lived Contraction of the WPWP Southern Edge at 6.2–6.0 ka BP

[34] The 6.2–6.0 ka BP *Tridacna maxima* record revealed that the SW Pacific experienced slight SST fluctuations during the post-glacial stabilization of the SST around its present values. Because the modern New Caledonian giant clam and the fossil Vanuatu giant clam mean $\delta^{18}O$ values are similar, they may have grown in similar environmental conditions. Considering that New Caledonia surface water is on average ~3.5°C cooler and ~0.5 saltier compared to the Vanuatu ones (Figure 3), conditions in the Vanuatu region at around 6.2–6.0 ka BP were most likely cooler and saltier than today.

[35] However, a SST drop of ~3.5°C at 6.2–6.0 ka BP is very unlikely considering that the two fossil coral records from Vanuatu showed mean SST values similar to modern ones at 6.7–6.5 ka BP. This SST drop is thus most likely overestimated. The two fossil coral $\delta^{18}O$ records revealed that the seawater was enriched in the heavier oxygen isotope by +0.3‰ vpdb indicating saltier than present mean conditions at 6.7–6.5 ka BP (Figure 7). Assuming that the $\delta^{18}O_{sw}$ recorded by the fossil corals remain unchanged at 6.2–6.0 ka BP, such seawater ^{18}O enrichment would have shifted the giant clam shell $\delta^{18}O$ value in the same proportion, because giant clam aragonite is deposited in isotopic equilibrium with seawater. Considering an average $\delta^{18}O$ versus SST slope

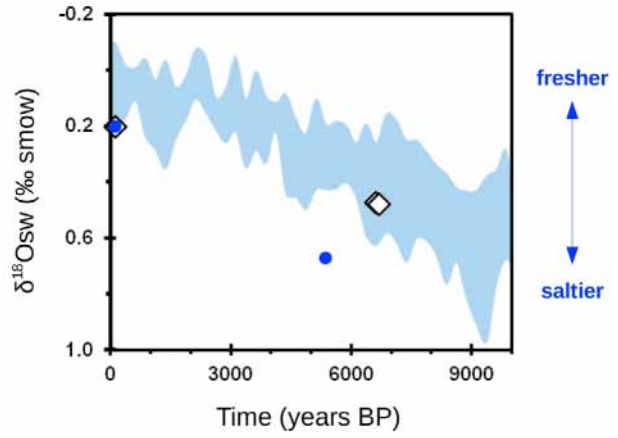

Figure 9. Holocene $\delta^{18}O_{sw}$ evolution in the Western Pacific area – Diamond: coral data (this study), Blue dots: coral data from *Gagan et al.* [1998]. Blue area – foraminifer's data from sediment cores ODP806B, MD70, MD76 and MD81. The blue area represents one standard deviation interval of the mean values calculated from the four sedimentary records [*Lea et al.*, 2000; *Stott et al.*, 2004].

of 0.26‰.C°$^{-1}$ for Tridacnidae shells [*Aharon*, 1980; *Watanabe and Oba*, 1999; *Aubert et al.*, 2009], the SSS change in the early mid-Holocene would account for an apparent SST cooling of about 1°C. In addition, the equations linking giant clam $\delta^{18}O$ to SST show that the accuracy of this proxy is between ±1°C and ±1.4°C [*Watanabe and Oba*, 1999; *Aubert et al.*, 2009]. This accuracy of giant clam $\delta^{18}O$ as a temperature proxy must also be considered and could explain this overestimated SST change. The SST negative anomaly recorded by the fossil giant clam is thus most probably around 2 ± 1°C. This value is consistent with the 1–2°C cooling observed ca. 6.0 ka BP at the margins of the IPWP by *Abram et al.* [2009]. According to *Lea et al.* [2000] and *Stott et al.* [2004], the SST in the western equatorial Pacific during the Holocene presented weak variations around the modern SST values. Colder conditions observed at the southern edge of the WPWP at 6.2–6.0 ka BP are thus probably not related to a cooling trend of the WPWP, but rather to a short-lived contraction or northward migration of the WPWP. This suggests that the southern edge of the WPWP retracted below its actual boundaries at that time. Such fluctuation of the WPWP' southern edge during the Holocene is also suggested by the planktonic foraminifera $\delta^{18}O$ record from the Ocean Drilling Program sediment core 828A, collected offshore Vanuatu [*Martinet et al.*, 1997]. Interestingly, the timing of this event matches the global cooling event reported at around 6.3 ka BP [see the review in *Wanner et al.*, 2011]. However, additional mid-Holocene paleo-SST records in the Vanuatu region are needed to confirm the timing of such a northward shift of the WPWP at 6.2–6.0 ka BP and to determine to which extent the SW Pacific cooling may be linked to this global cold event.

5.3. Early Mid-Holocene Surface-Ocean Water Balance

[36] The post-glacial stabilization of SST around its present value in the SW Pacific at 6.7–6.5 ka BP was accompanied by change of the surface-ocean water balance compared to modern conditions. The modern coral record from Vanuatu displays a low average $\delta^{18}O_{sw}$ value (0.0‰ vpdb) that reflects the strong influence of ^{18}O-depleted waters brought by the SPCZ-related precipitation (Figure 3). The modern coral record shows a positive $\delta^{18}O_{sw}$ peak in October linked to a reduction in precipitation input (Figure 7a). Indeed, Vanuatu is not influenced by the SPCZ in winter (Figure 2b) and the increased easterlies in winter induce a strong evaporation that contributes to enrich the surface seawater with the heavier oxygen isotope. This $\delta^{18}O_{sw}$ peak reflects a higher SSS in agreement with the instrumental record (Figure 3). As such, any change of the surface-ocean water balance (i.e., SSS) would be recorded in the early mid-Holocene coral $\delta^{18}O_{sw}$ profiles.

[37] The early mid-Holocene corals recorded an average $\delta^{18}O_{sw}$ composition enriched by about +0.3‰ vpdb compared to the modern seawater (Figure 7). The early mid-Holocene average $\delta^{18}O_{sw}$ composition is similar to the modern winter value, suggesting that the average surface-ocean water balance at ca. 6.7–6.5 ka BP was shifted toward modern winter-like conditions, i.e., when the SPCZ is not affecting the Vanuatu region (Figure 2b). Such a dramatic reduction of SPCZ-related precipitation input indicates that the SPCZ was most likely located northward from its present location and possibly merged with the inter tropical convergence zone. Moreover, the seasonal $\delta^{18}O_{sw}$ cycle reveals that the early mid-Holocene summers were characterized by saltier conditions whereas fresher conditions would have been expected regarding the southward summer migration of the SPCZ observed today (Figure 2b). This supports the assumption of a northerly located SPCZ during the early mid-Holocene.

[38] However, these results seem in contradiction with numerical climate simulations at 6 ka BP that evidenced a southward shift, and an intensification, of the SPCZ [*Brown et al.*, 2007, 2008; *Chiang et al.*, 2009]. It may be argued that saltier conditions recorded by the fossil corals during the early mid-Holocene summers may reflect the occurrence of seasonal upwelling that could have counter-balanced the SSS dilution due to SPCZ-related precipitation in the SW Pacific. Nevertheless, the water masses located beneath the thermocline are characterized by higher SSS and lower SST than superficial waters [*Maes and Varillon*, 2011], so that a seasonally easterlies-driven upwelling regime in the SW Pacific would have led to opposite reconstructed SSS and SST variations. Consequently, the dramatic precipitation deficit and dry summers during the early mid-Holocene strongly suggest that the precipitation regime was decoupled from the SPCZ during the early mid-Holocene. Fossil coral records would thus reflects local variations of the precipitation regime rather than variations of the SPCZ location or intensity.

[39] The northerly located SPCZ during the early mid-Holocene as demonstrated in this study is consistent with the northward location of the ITCZ during the early mid-Holocene evidenced from sediment proxy data [*Haug et al.*, 2001] and from coupled ocean-atmosphere model simulations [*Braconnot et al.*, 2007]. This suggests a synchronous northward displacement of both the ITCZ and the SPCZ during the early mid-Holocene, explaining the high SSS observed in the Western Pacific during the first half of the Holocene (Figure 9). These observations evidence that the Pacific Ocean convective features experienced an important northward re-organization during the early mid-Holocene, possibly in response to the orbital forcing.

[40] However, the northward location of the SPCZ solely cannot explain the salinity recorded in summer by the early mid-Holocene corals. Indeed, this summer $\delta^{18}O_{sw}$ value reaches 0.5‰ vpdb which indicates even drier conditions than recorded today during winter (0.3‰ vpdb – Figure 7), when Vanuatu is not affected by the SPCZ. This suggests that evaporation had also played a significant role in the surface-ocean water balance during the early mid-Holocene. An average surface-ocean water balance shifted toward evaporation during the mid-Holocene was shown from a Australian Great Barrier Reef coral record [*Gagan et al.*, 1998]. Increased evaporation in the early mid-Holocene is also supported by the similar or warmer conditions than today recorded by early mid-Holocene fossil corals from PNG, GBR, and New Caledonia [*Gagan et al.*, 1998, 2004; *Montaggioni et al.*, 2006; *Abram et al.*, 2009]. Moreover, general circulation model simulations indicate a strengthening, or an extension, of the Hadley cell as a response of a slight warming of the tropical zone [*Rind*, 2000; *Lu et al.*, 2007]. Stronger, or extended, Hadley cell would enhance the poleward water vapor transport, and thus the poleward heat flux, increasing the evaporation in the tropics. This suggests a stronger coupling between the tropics and the extra-tropical regions during the early mid-Holocene as compared to the modern era.

5.4. ENSO Variability

[41] Since coral $\delta^{18}O$ is sensitive to both SST and SSS variations, it is a reliable proxy to study the ENSO variability. Indeed, a synchronous increase (decrease) in SST and decrease (increase) in SSS influences the coral $\delta^{18}O$ in the same way, resulting in enhanced interannual coral $\delta^{18}O$ variations as observed in the modern Vanuatu coral record (Figure 8a). The early mid-Holocene coral from Vanuatu recorded a ENSO variability that was in average 20–30% lower than the variability recorded by the modern coral for the period 1928–1992 (Figure 8b).

[42] Several factors may have caused the ENSO variability to weaken during the early mid-Holocene. On the one hand, previous studies suggested that ENSO teleconnections may not be stationary [e.g., *Stahle et al.*, 1998; *Diaz et al.*, 2001; *Vargas et al.*, 2006]. Consequently, a change in the ENSO teleconnections over the Pacific area during the early mid-Holocene may result in a reduced ENSO signal in the SW Pacific fossil corals records. On the other hand, the decoupling between the precipitation and the SPCZ in the SW Pacific, evidenced from the early mid-Holocene coral records, may also have contributed to a reduced ENSO signal in the $\delta^{18}O$ coral record. Indeed, the strength of the ENSO signal in the coral $\delta^{18}O$ record relies on the tight coupling between the SPCZ and the precipitation. The decoupling of the SPCZ and the precipitation regime observed during the early mid-Holocene would have lead to a disruption between the ENSO variability and coral $\delta^{18}O$ variations, leading to a weaker ENSO signal in the $\delta^{18}O$ record.

[43] Non stationary ENSO teleconnections in the SW Pacific, or a decoupling between the precipitation and ENSO would thus appear as locally reduced ENSO variability while stronger ENSO variability prevails in the regions where ENSO is tightly linked to, i.e., the WPWP, the Pacific cold tongue or western South America. However, paleo reconstructions from PNG charcoal and coral records revealed a significant reduction of the ENSO variability during the early mid-Holocene [*Haberle et al.*, 2001; *Tudhope et al.*, 2001]. Moreover, mollusks, archeological and sedimentary records from South America and the cold tongue area evidenced a reduced ENSO variability during the early and the early mid-Holocene [*Sandweiss et al.*, 2001; *Moy et al.*, 2002; *Koutavas et al.*, 2006; *Vargas et al.*, 2006]. Weak ENSO variability during the first half of the Holocene is also observed in ocean-atmosphere coupled model runs. All those evidences strongly suggest that the reduced ENSO variability recorded by the early mid-Holocene Vanuatu coral reflects a real ENSO trend, although the role of the forcing involved in the ENSO variability decrease are still greatly debated [*Clement et al.*, 2000; *Liu et al.*, 2000; *Roberts*, 2007; *Zheng et al.*, 2008; *Chiang et al.*, 2009; *Braconnot et al.*, 2012]. Consequently, the reduced amplitude of the ENSO signal in the early mid-Holocene coral $\delta^{18}O$ record reflect both 1) a global weaker ENSO variability and 2) the decoupling between the precipitation and the SPCZ.

6. Conclusion

[44] Monthly resolved $\delta^{18}O$ records from two 6.7–6.5 ka BP *Porites sp.* colonies and from a 6.2–6.0 ka BP *Tridacna maxima* opened a window on the SW Pacific climate during the early mid-Holocene. The post-glacial SST rise was found to be completed by about 6.7–6.5 ka BP with conditions as warm, or slightly higher, than today suggesting a weak Holocene Thermal Maximum in that region. Cooler conditions were recorded at 6.2–6.0 ka BP, possibly related to a short-lived contraction of the WPWP southern edge. Early mid-Holocene *Porites sp.* records revealed drier than modern conditions, caused by a northward mean position of the SPCZ and an increased moisture transport in the extra tropics related to a strengthened or extended Hadley circulation. Such configuration strongly suggests that the climatic mean state was La Niña-like during the early mid-Holocene period.

[45] One of the early mid-Holocene corals recorded a lower ENSO variability than the modern one. This reflects the reduced ENSO variability evidenced by previous studies during the first half of the Holocene, although the decoupling between the SPCZ and the precipitation regime in the SW Pacific may also have contributed to the reduced ENSO signal observed in our coral record. The combined use of corals and of a giant clam improves the temporal and spatial coverage of early mid-Holocene data in the SW Pacific area. The information brought by our study provides an benchmark against which to test climate models and should help constraining the SPCZ behavior in simulations of past and modern climate conditions.

[46] **Acknowledgments.** We thank Richard Farman and the Aquarium des Lagons of Nouméa (New Caledonia) for the raceway facilities. We also thank the owner of the Ratua Island resort and Jean-Christophe Galipaud for their help in the fossils collection, Rufino Pineda for the logistical help in Espiritu Santo, and John Butscher for the logistical help in New Caledonia. We are also grateful to the radiology staff of Jean Verdier Hospital (Bondy, Seine Saint Denis, France) for coral slabs x-radiographs. Thanks are extended to Hugues Boucher for the data processing. Marielle Dumestre, Joël Ughetto also contributed to many helpful discussions. The authors are grateful to Gavin Dunbar and to an anonymous reviewer for their corrections and comments, which help improving that manuscript. This study was done in the framework of the HOLBECO project, supported by the French INSU-EC2CO program (managed by the IFREMER Institute). This work is dedicated to our esteemed and dearly missed colleague Guy Cabioch.

References

Abram, N. J., H. V. McGregor, M. K. Gagan, W. S. Hantoro, and B. W. Suwargadi (2009), Oscillations in the southern extent of the Indo-Pacific Warm Pool during the mid-Holocene, *Quat. Sci. Rev.*, *28*(25–26), 2794–2803, doi:10.1016/j.quascirev.2009.07.006.

Aharon, P. (1980), Stable isotope geochemistry of a late quaternary coral reef sequence, New Guinea: Application of high resolution data to paleoclimatology, PhD thesis, Australian National Univ., Canberra, ACT, Australia.

Ambrizzi, T., B. J. Hoskins, and H.-H. Hsu (1995), Rossby Wave Propagation and Teleconnection Patterns in the Austral Winter, *J. Atmos. Sci.*, *52*(21), 3661–3672, doi:10.1175/1520-0469(1995)052<3661:RWPATP>2.0.CO;2.

Aubert, A., C. E. Lazareth, G. Cabioch, H. Boucher, T. Yamada, Y. Iryu, and R. Farman (2009), The tropical giant clam *Hippopus hippopus* shell, a new archive of environmental conditions as revealed by sclerochronological and $\delta^{18}O$ profiles, *Coral Reefs*, *28*(4), 989–998, doi:10.1007/s00338-009-0538-0.

Beck, J. W. (1997), Abrupt changes in early Holocene tropical sea surface temperature from coral Sr/Ca thermometry, *Nature*, *385*, 705–707, doi:10.1038/385705a0.

Beck, J. W., R. L. Edwards, E. Ito, F. W. Taylor, J. Recy, F. Rougerie, P. Joannot, and C. Henin (1992), Sea-surface temperature from coral skeletal strontium/calcium ratios, *Science*, *257*(5070), 644–647, doi:10.1126/science.257.5070.644.

Berger, A., and M. F. Loutre (1991), Insolation values for the climate of the last 10 million years, *Quat. Sci. Rev.*, *10*(4), 297–317, doi:10.1016/0277-3791(91)90033-Q.

Braconnot, P., et al. (2007), Results of PMIP2 coupled simulations of the Mid-Holocene and Last Glacial Maximum – Part 2: Feedbacks with emphasis on the location of the ITCZ and mid- and high latitudes heat budget, *Clim. Past*, *3*(2), 279–296, doi:10.5194/cp-3-279-2007.

Braconnot, P., Y. Luan, S. Brewer, and W. Zheng (2012), Impact of Earth's orbit and freshwater fluxes on Holocene climate mean seasonal cycle and ENSO characteristics, *Clim. Dyn.*, *38*(5–6), 1081–1092, doi:10.1007/s00382-011-1029-x.

Brown, J., M. Collins, A. W. Tudhope, and T. Toniazzo (2007), Modeling mid-Holocene tropical climate and ENSO variability: Towards constraining predictions of future change with palaeo-data, *Clim. Dyn.*, *30*(1), 19–36, doi:10.1007/s00382-007-0270-9.

Brown, J., A. W. Tudhope, M. Collins, and H. V. McGregor (2008), Mid-Holocene ENSO: Issues in quantitative model-proxy data comparisons, *Paleoceanography*, *23*, PA3202, doi:10.1029/2007PA001512.

Cane, M. A. (2005), The evolution of El Niño, past and future, *Earth Planet. Sci. Lett.*, *230*(3–4), 227–240, doi:10.1016/j.epsl.2004.12.003.

Cane, M., and A. C. Clement (1999), A role for the tropical Pacific coupled ocean-atmosphere system on Milankovitch and millennial timescales part II: Global impacts, in *Mechanisms of Global Climate Change at Millennial Time Scales*, *Geophys. Monogr. Ser*, vol. 112, edited by U. Clark, S. Webb, and D. Keigwin, pp. 373–383, AGU, Washington, D. C., doi:10.1029/GM112p0373.

Chiang, J. C. H., Y. Fang, and P. Chang (2009), Pacific climate change and ENSO activity in the Mid-Holocene, *J. Clim.*, *22*(4), 923–939, doi:10.1175/2008JCLI2644.1.

Clement, A. C., R. Seager, and M. A. Cane (2000), Suppression of El Niño during the mid-Holocene by changes in the Earth's orbit, *Paleoceanography*, *15*(6), 731–737, doi:10.1029/1999PA000466.

Corrège, T. (2006), Sea surface temperature and salinity reconstruction from coral geochemical tracers, *Palaeogeogr. Palaeoclimatol. Palaeoecol.*, *232*(2–4), 408–428, doi:10.1016/j.palaeo.2005.10.014.

deMenocal, P., J. Ortiz, T. Guilderson, J. Adkins, M. Sarnthein, L. Baker, and M. Yarusinsky (2000), Abrupt onset and termination of the African Humid Period: Rapid climate responses to gradual insolation forcing, *Quat. Sci. Rev.*, *19*, 347–361, doi:10.1016/S0277-3791(99)00081-5.

Diaz, H. F., M. P. Hoerling, and J. K. Eischeid (2001), ENSO variability, teleconnections and climate change, *Int. J. Climatol.*, *21*(15), 1845–1862, doi:10.1002/joc.631.

Elliot, M., K. Welsh, C. Chilcott, M. McCulloch, J. Chappell, and B. Ayling (2009), Profiles of trace elements and stable isotopes derived from giant long-lived *Tridacna gigas* bivalves: Potential applications in paleoclimate studies, *Palaeogeogr. Palaeoclimatol. Palaeoecol.*, *280*(1–2), 132–142, doi:10.1016/j.palaeo.2009.06.007.

Gagan, M. K., L. K. Ayliffe, D. Hopley, J. A. Cali, G. E. Mortimer, J. Chappell, M. T. McCulloch, and M. J. Head (1998), Temperature and surface-ocean water balance of the mid-Holocene tropical Western Pacific, *Science*, *279*(5353), 1014–1018, doi:10.1126/science.279.5353.1014.

Gagan, M. K., E. J. Hendy, S. G. Haberle, and W. S. Hantoro (2004), Post-glacial evolution of the Indo-Pacific Warm Pool and El Niño-Southern Oscillation, *Quat. Int.*, *118–119*, 127–143, doi:10.1016/S1040-6182(03)00134-4.

Gouriou, Y., and T. Delcroix (2002), Seasonal and ENSO variations of sea surface salinity and temperature in the South Pacific Convergence Zone during 1976–2000, *J. Geophys. Res.*, *107*(C12), 3185, doi:10.1029/2001JC000830.

Haberle, S. G., G. S. Hope, and S. van der Kaars (2001), Biomass burning in Indonesia and Papua New Guinea: Natural and human induced fire events in the fossil record, *Palaeogeogr. Palaeoclimatol. Palaeoecol.*, *171*(3–4), 259–268, doi:10.1016/S0031-0182(01)00248-6.

Hathorne, E., et al. (2010), An inter-laboratory study of coral Sr/Ca and other element/Ca ratios, poster presented at 10th International Conference on Paleoceanography, ICP 10, La Jolla, Calif.

Haug, G. H., K. A. Hughen, D. M. Sigman, L. C. Peterson, and U. Rohl (2001), Southward migration of the intertropical convergence zone through the Holocene, *Science*, *293*(5533), 1304–1308, doi:10.1126/science.1059725.

Inoue, M., M. Nohara, T. Okai, A. Suzuki, and H. Kawahata (2004), Concentrations of trace elements in carbonate reference materials coral JCp-1 and giant clam JCt-1 by inductively coupled plasma-mass spectrometry, *Geostand. Geoanal.Res.*, *28*(3), 411–416, doi:10.1111/j.1751-908X.2004.tb00759.x.

Juillet-Leclerc, A., and G. Schmidt (2001), A calibration of the oxygen isotope paleothermometer of coral aragonite from *Porites*, *Geophys. Res. Lett.*, *28*(21), 4135–4138, doi:10.1029/2000GL012538.

Juillet-Leclerc, A., S. Thiria, P. Naveau, T. Delcroix, N. Le Bec, D. Blamart, and T. Corrège (2006), SPCZ migration and ENSO events during the 20th century as revealed by climate proxies from a Fiji coral, *Geophys. Res. Lett.*, *33*, L17710, doi:10.1029/2006GL025950.

Kaplan, A., M. A. Cane, Y. Kushnir, A. C. Clement, M. B. Blumenthal, and B. Rajagopalan (1998), Analyses of global sea surface temperature 1856–1991, *J. Geophys. Res.*, *103*(C9), 18,567–18,589.

Kiladis, G. N., and H. F. Diaz (1989), Global climatic anomalies associated with extremes in the Southern Oscillation, *J. Clim.*, *2*(9), 1069–1090, doi:10.1175/1520-0442(1989)002<1069:GCAAWE>2.0.CO;2.

Kiladis, G. N., H. Vonstorch, and H. Vanloon (1989), Origin of the South-Pacific Convergence Zone, *J. Clim.*, *2*(10), 1185–1195, doi:10.1175/1520-0442(1989)002<1185:OOTSPC>2.0.CO;2.

Kilbourne, K. H., T. M. Quinn, F. W. Taylor, T. Delcroix, and Y. Gouriou (2004), El Niño-Southern Oscillation-related salinity variations recorded in the skeletal geochemistry of a *Porites* coral from Espiritu Santo, Vanuatu, *Paleoceanography*, *19*, PA4002, doi:10.1029/2004PA001033.

Knutson, D. W. (1972), Coral chronometers: Seasonal growth bands in reef corals, *Science*, *177*, 270–272, doi:10.1126/science.177.4045.270.

Koutavas, A., P. B. Demenocal, G. C. Olive, and J. Lynch-Stieglitz (2006), Mid-Holocene El Niño-Southern Oscillation (ENSO) attenuation revealed by individual foraminifera in eastern tropical Pacific sediments, *Geology*, *34*(12), 993–996, doi:10.1130/G22810A.1.

Le Borgne, R., R. T. Barber, T. Delcroix, H. Y. Inoue, D. J. Mackey, and M. Rodier (2002), Pacific warm pool and divergence: Temporal and zonal variations on the equator and their effects on the biological pump, *Deep Sea Res., Part II*, *49*(13–14), 2471–2512, doi:10.1016/S0967-0645(02)00045-0.

Le Cornec, F., and T. Corrège (1997), Determination of uranium to calcium and strontium to calcium ratios in corals by Inductively Coupled Plasma Mass Spectrometry, *J. Anal. At. Spectrom.*, *12*(9), 969–973, doi:10.1039/a701691c.

Lea, D. W., D. K. Pak, and H. J. Spero (2000), Climate impact of Late Quaternary equatorial Pacific sea surface temperature variations, *Science*, *289*(5485), 1719–1724, doi:10.1126/science.289.5485.1719.

Liu, Z., I. Kutzbach, and L. Wu (2000), Modeling climate shift of E1 Niño variability in the Holocene, *Geophys. Res. Lett.*, *27*(15), 2265–2268, doi:10.1029/2000GL011452.

Lu, J., G. A. Vecchi, and T. Reichler (2007), Expansion of the Hadley cell under global warming, *Geophys. Res. Lett.*, *34*, L06805, doi:10.1029/2006GL028443.

Lyon, B. (2004), The strength of El Niño and the spatial extent of tropical drought, *Geophys. Res. Lett.*, *31*, L21204, doi:10.1029/2004GL020901.

Maes, C., and D. Varillon (2011), Large-scale climatic and oceanic conditions around Santo, in *The Natural History of Santo*, edited by P. Bouchet, H. Le Guyader, and O. Pascal, pp. 57–61, Muséum national d'Histoire naturelle, Paris.

Maes, C., J. Sudre, and V. Garçon (2010), Detection of the eastern edge of the Equatorial Pacific Warm Pool using satellite-based ocean color observations, *SOLA*, *6*, 129–132, doi:10.2151/sola.2010-033.

Martinet, J. I., P. D. Deckker, and A. R. Chivas (1997), New estimates for salinity changes in the Western Pacific Warm Pool during the Last Glacial Maximum: Oxygen-isotope evidence, *Mar. Micropaleontol.*, *32*(3–4), 311–340, doi:10.1016/S0377-8398(97)00029-7.

McConnaughey, T. (1989), C-13 and O-18 isotopic disequilibrium in biological carbonates.2. invitro simulation of kinetic isotope effects,

Geochim. Cosmochim. Acta, *53*(1), 163–171, doi:10.1016/0016-7037(89)90283-4.

McPhaden, M. J., S. E. Zebiak, and M. H. Glantz (2006), ENSO as an integrating concept in earth science, *Science*, *314*(5806), 1740–1745, doi:10.1126/science.1132588.

Montaggioni, L. F., F. Le Cornec, T. Corrège, and G. Cabioch (2006), Coral barium/calcium record of mid-Holocene upwelling activity in New Caledonia, South-West Pacific, *Palaeogeogr. Palaeoclimatol. Palaeoecol.*, *237*(2–4), 436–455, doi:10.1016/j.palaeo.2005.12.018.

Morimoto, M., O. Abe, H. Kayanne, N. Kurita, E. Matsumoto, and N. Yoshida (2002), Salinity records for the 1997–98 El Niño from Western Pacific corals, *Geophys. Res. Lett.*, *29*(11), 1540, doi:10.1029/2001GL013521

Moy, C. M., G. O. Seltzer, D. T. Rodbell, and D. M. Anderson (2002), Variability of El Niño/Southern Oscillation activity at millennial timescales during the Holocene epoch, *Nature*, *420*(6912), 162–165, doi:10.1038/nature01194.

Okai, T., A. Suzuki, H. Kawahata, S. Terashima, and N. Imai (2002), Preparation of a new geological survey of Japan geochemical reference material: Coral JCp-1, *Geostand. Newsl.*, *26*(1), 95–99, doi:10.1111/j.1751-908X.2002.tb00627.x.

Petchey, F., A. Anderson, A. Zondervan, S. Ulm, and A. Hogg (2008), New marine deltaR values for the South Pacific subtropical gyre region, *Radiocarbon*, *50*(3), 373–397.

Picaut, J., M. Ioualalen, T. Delcroix, F. Masia, R. Murtugudde, and J. Vialard (2001), The oceanic zone of convergence on the eastern edge of the Pacific warm pool: A synthesis of results and implications for El Niño-Southern Oscillation and biogeochemical phenomena, *J. Geophys. Res.*, *106*(C2), 2363–2386, doi:10.1029/2000JC900141.

Rayner, N. A., D. E. Parker, E. B. Horton, C. K. Folland, L. V. Alexander, D. P. Rowell, E. C. Kent, and A. Kaplan (2003), Global analyses of sea surface temperature, sea ice, and night marine air temperature since the late nineteenth century, *J. Geophys. Res.*, *108*(D14), 4407, doi:10.1029/2002JD002670.

Reimer, P. J., et al. (2009), Intcal09 and Marine09 radiocarbon age calibration curves, 0–50,000 Years Cal Bp, *Radiocarbon*, *51*(4), 1111–1150.

Renssen, H., H. Seppä, X. Crosta, H. Goosse, and D. M. Roche (2012), Global characterization of the Holocene Thermal Maximum, *Quat. Sci. Rev.*, *48*, 7–19, doi:10.1016/j.quascirev.2012.05.022.

Rind, D. (2000), Relating paleoclimate data and past temperature gradients: Some suggestive rules, *Quat. Sci. Rev.*, *19*, 381–390, doi:10.1016/S0277-3791(99)00070-0.

Roberts, W. H. (2007), An investigation into the causes for the reduction in the variability of the El Niño Southern Oscillation in the early Holocene in a global climate model, PhD thesis, Univ. of Washington, Seattle.

Sandweiss, D. H., K. A. Maasch, R. L. Burger, J. B. Richardson III, H. B. Rollins, and A. Clement (2001), Variation in Holocene El Niño frequencies: Climate records and cultural consequences in ancient Peru, *Geology*, *29*(7), 603–606, doi:10.1130/0091-7613(2001)029<0603:VIHENO>2.0.CO;2.

Schneider, R. C., and S. V. Smith (1982), Skeletal Sr content and density in *Porites* spp. in relation to environmental factors, *Mar. Biol. Berlin*, *66*(2), 121–131, doi:10.1007/BF00397185.

Stahle, D. W., et al. (1998), Experimental dendroclimatic reconstruction of the Southern Oscillation, *Bull. Am. Meteorol. Soc.*, *79*, 2137–2152, doi:10.1175/1520-0477(1998)079<2137:EDROTS>2.0.CO;2.

Stott, L., K. Cannariato, R. Thunell, G. H. Haug, A. Koutavas, and S. Lund (2004), Decline of surface temperature and salinity in the western tropical Pacific Ocean in the Holocene epoch, *Nature*, *431*(7004), 56–59, doi:10.1038/nature02903.

Swart, P. K. (1981), The strontium, magnesium and sodium composition of recent scleractinian coral skeletons as standards for palaeoenvironmental analysis, *Palaeogeogr. Palaeoclimatol. Palaeoecol.*, *34*(0), 115–136, doi:10.1016/0031-0182(81)90060-2.

Taylor, T. W. (1992), Quaternary vertical tectonics of the central New Hebrides island arc, *Proc. Ocean Drill. Program Initial Rep., 134*, 47–57, Ocean Drill. Program, College Station, Tex.

Trenberth, K. E. (1976), Spatial and temporal variations of Southern Oscillation, *Q. J. R. Meteorol. Soc.*, *102*(433), 639–653, doi:10.1002/qj.49710243310.

Tudhope, A. W., C. P. Chilcott, M. T. McCulloch, E. R. Cook, J. Chappell, R. M. Ellam, D. W. Lea, J. M. Lough, and G. B. Shimmield (2001), Variability in the El Niño—Southern oscillation through a glacial-interglacial cycle, *Science*, *291*(5508), 1511–1517, doi:10.1126/science.1057969.

Vargas, G., J. Rutllant, and L. Ortlieb (2006), ENSO tropical-extratropical climate teleconnections and mechanisms for Holocene debris flows along the hyperarid coast of western South America (17 degrees-24 degrees S), *Earth Planet. Sci. Lett.*, *249*(3–4), 467–483, doi:10.1016/j.epsl.2006.07.022.

Vincent, D. G. (1994), The South-Pacific Convergence Zone (SPCZ) – A review, *Mon. Weather Rev.*, *122*(9), 1949–1970, doi:10.1175/1520-0493(1994)122<1949:TSPCZA>2.0.CO;2.

Wang, P., S. Clemens, L. Beaufort, P. Braconnot, G. Ganssen, Z. Jian, P. Kershaw, and M. Sarnthein (2005), Evolution and variability of the Asian monsoon system: State of the art and outstanding issues, *Quat. Sci. Rev.*, *24*(5–6), 595–629, doi:10.1016/j.quascirev.2004.10.002.

Wanner, H., et al. (2008), Mid- to Late Holocene climate change: An overview, *Quat. Sci. Rev.*, *27*(19–20), 1791–1828, doi:10.1016/j.quascirev.2008.06.013.

Wanner, H., O. Solomina, M. Grosjean, S. P. Ritz, and M. Jetel (2011), Structure and origin of Holocene cold events, *Quat. Sci. Rev.*, *30*(21–22), 3109–3123, doi:10.1016/j.quascirev.2011.07.010.

Watanabe, T., and T. Oba (1999), Daily reconstruction of water temperature from oxygen isotopic ratios of a modern *Tridacna* shell using a freezing microtome sampling technique, *J. Geophys. Res.*, *104*(C9), 20,667–20,674, doi:10.1029/1999JC900097.

Wyrtki, K. (1989), Some thoughts about the west Pacific warm pool, in *Proceedings of the Western Pacific International Meeting and Workshop on TOGA COARE*, edited by J. Picaut, R. Lukas, and T. Delcroix, pp. 99–109, ORSTOM, Nouméa, New Caledonia.

Zhang, J. W., F. H. Chen, J. A. Holmes, H. Li, X. Y. Guo, J. L. Wang, S. Li, Y. B. Lu, Y. Zhao, and M. R. Qiang (2011), Holocene monsoon climate documented by oxygen and carbon isotopes from lake sediments and peat bogs in China: A review and synthesis, *Quat. Sci. Rev.*, *30*(15–16), 1973–1987, doi:10.1016/j.quascirev.2011.04.023.

Zheng, W., P. Braconnot, E. Guilyardi, U. Merkel, and Y. Yu (2008), ENSO at 6 ka and 21 ka from ocean–atmosphere coupled model simulations, *Clim. Dyn.*, *30*(7–8), 745–762, doi:10.1007/s00382-007-0320-3.